Hindawi
International Journal of Antennas and Propagation
Volume 2022, Article ID 2002552, 12 pages
https://doi.org/10.1155/2022/2002552

Research Article

Improvement in the Gain of UWB Antenna for GPR Applications by Using Frequency-Selective Surface

Iftikhar Ud Din,[1] Sadiq Ullah,[1] Syeda Iffat Naqvi,[2] Raza Ullah,[1] Shakir Ullah,[1] Esraa Mousa Ali,[3] and Mohammad Alibakhshikenari[4]

[1]*Department of Telecommunication Engineering, University of Engineering and Technology, Mardan 23200, Pakistan*
[2]*ACTSENA Research Group, Department of Telecommunication Engineering, University of Engineering and Technology, Taxila 47050, Punjab, Pakistan*
[3]*Faculty of Aviation Sciences, Amman Arab University, Amman 11953, Jordan*
[4]*Department of Signal Theory and Communications, Universidad Carlos III de Madrid, Leganés, 28911 Madrid, Spain*

Correspondence should be addressed to Sadiq Ullah; sadiqullah@uetmardan.edu.pk and Mohammad Alibakhshikenari; mohammad.alibakhshikenari@uc3m.es

Received 29 June 2022; Revised 30 September 2022; Accepted 10 October 2022; Published 29 October 2022

Academic Editor: Rajkishor Kumar

In this article, high-gain ultra-wideband (UWB) monopole antenna is presented. The UWB monopole antenna is a semicircular-shaped antenna with a semicircular slot at the top side. The bottom plane consists of partial ground with triangular and rectangular slotted structures to improve the impedance bandwidth of the proposed antenna. In order to enhance gain, a 6×6 metallic reflector (FSS) is placed below the antenna. The performance of the offered design is validated experimentally. The simulated results show resemblance with the measured results. The antenna resonates for the UWB ranging from 3 to 11 GHz. Moreover, the integration of FSS improves the average gain by 4 dB, where peak gain obtained is 8.3 dB across the UWB. In addition, the reported unit cell having dimension of $0.11\lambda \times 0.11\lambda$ gives wide bandwidth (7.2 GHz) from 3.3 GHz to 10.5 GHz. The performance of the proposed antenna determines its suitability for the modern day wireless UWB and GPR applications.

1. Introduction

Currently, ultra-wideband (UWB) technology has appeared as an auspicious candidate for both military and commercial wireless communication applications [1, 2]. UWB technology has various applications such as multimedia for home entertainment, sensor networks, and personal computer industry. It is also useful for physical layer protocols for high transmission IEEE 802.15.3 and low transmission IEEE 802.15.4 standards [3]. The allocated spectrum for UWB communication by Federal Communication Commission (FCC) ranges from 3.1 to 10.6 GHz. Due to promising radiation characteristics such as large bandwidth, higher data rate, and minimal power requirement, the UWB antennas have been widely used in applications like precision locating, tracking applications, radar imaging, and various other commercial applications [4–8]. The antenna reported in [4] has compact size, wide bandwidth, and high gain and has applications in the area of human microwave imaging. In [5], the proposed antenna is used for multiple wireless applications covering wideband from 2.3 to 20 GHz especially for Wi-Fi and Ku band. Similarly, a compact slotted UWB is designed for various medical imaging and polarimetric radar applications [6]. Likewise, an UWB antenna is demonstrated in [7] for specific ground-penetrating radar (GPR) detection applications. The UWB antenna proposed in [8] has band notch characteristics with reconfigurable single and dual band characteristics. Thus, contribution of UWB antennas towards these significant applications motivated the researchers towards further investigation of the UWB antennas. To obtain UWB performance, various design techniques such as slotted patch

antennas with partial and slotted ground plane, stubs in the ground, and monopole antennas with rectangular, U-shaped, circular, elliptical, and even more complex structures have been frequently reported in the literature [9–15]. In [9, 10], circular and elliptical-shaped antennas are proposed covering UWB spectrum. The work in [11] reported a rectangular-shaped UWB antenna with an inverted T-shaped notch at the bottom to improve the bandwidth ranging from 3.12 to 12.73 GHz. Likewise, elliptical UWB antennas are presented in [12, 13] with a slotted ground plane to enhance the radiation characteristics of the antenna. In the same way, the designs reported in [14, 15] incorporated slots in the ground plane to improve the impedance bandwidth of the UWB antenna. In addition to UWB characteristics, small-sized antennas are essential for compact wireless devices. Thus, several works have been reported recently with compact and low-profile antenna designs with UWB properties [16–18]. However, due to low profile, it is difficult for these antennas to attain high gain over the entire bandwidth and consequently UWB antennas have poor directivity.

On the other hand, some particular wireless communication applications such as location tracking, radar, and positioning systems necessitate highly directive antennas with high gain [19]. In order to enhance gain, various techniques have been investigated and hence reported in the literature such as defected ground structures (DGSs), dielectric resonator antennas (DRAs), array antennas, electromagnetic band gap structures (EBGs), and parasitic elements [20–23]. The antenna design reported in [20] introduced gate-like structures at the ground to achieve stable radiation pattern and high gain. In another work [21], a compact DRA is presented operating at UWB spectrum. Moreover, another UWB antenna with differential microstrip feed and triangular as well as trapezoidal-shaped DGS is proposed in [22]. Also, to improve gain, another double-layered UWB antenna is reported in [23].

In addition to abovementioned techniques, frequency-selective surfaces (FSSs) have recently drawn attention of researchers for gain improvement. Several literary works employed FSS for gain improvement [24–33]. The work in [24] proposed an UWB antenna with substrate dimensions of $30 \times 60\,\text{mm}^2$. For gain improvement, a two-layered FSS surface is employed, and hence a 3–4 dB improvement in gain is obtained. Similarly, the UWB antenna reported in [25] used a double split ring metasurface as a reflector to improve gain. An overall gain improvement of 5.5 dB is attained for this design. Another leaf-shaped UWB antenna is presented in [26] with overall dimensions of $40 \times 30\,\text{mm}^2$. This structure involves dual FSS layers to increase gain. As a result, an enhancement of 2–4.5 dBi in gain is achieved with overall peak gain of 8.7 dB. Likewise, another work [27] proposed two FSS reflector designs (FSS1 and FSS2) with overall dimensions of $82.5 \times 82.5\,\text{mm}^2$ an d $62.5 \times 62.5\,\text{mm}^2$, respectively, to increase the UWB antenna gain. An improvement of 2.5 and 2 dB in antenna gain is obtained for the proposed structures, respectively. The UWB antenna reported in [28] with geometrical dimensions of $41 \times 34\,\text{mm}^2$ employs a single-layered FSS for gain enhancement. This structure achieved an improvement of 2–3.5 dB in antenna gain with maximum gain of 7.6 dB over the entire resonant band. Moreover, another UWB antenna for microwave imaging applications is proposed in [29], where single-layered FSS is introduced to improve gain. Similarly, in [30], an UWB monopole antenna is reported where a gain enhancement of 4.5 dBi is achieved by employing single-layered FSS. The work in [31] presented another UWB monopole antenna for microwave radiology imaging and ground-penetrating radar applications, with FSS introduced as a reflecting layer to improve gain. In [32], an UWB patch antenna with tightly coupled FSS is proposed. In this work, squirrel search algorithm (SSA) is used to optimize the design parameters of the proposed design. Another work [33] reported a compact U-shaped UWB antenna with uniplanar FSS. The FSS improved the gain from 2.5 to 5.2 dBi in the operating band. It is observed that most of the previously reported works as discussed above are UWB antennas with double-layered FSS structures which increase not only the overall antenna size but also the fabrication complexity. These multilayered designs have limited practical applications due to their bulky structures. Moreover, the designs with single-layered FSS have low gain enhancement or have larger geometrical dimensions.

In order to deal with the abovementioned challenges associated with UWB antennas and to overcome limitations of the earlier reported works, this paper presents a FSS-based UWB antenna for wireless communication. The proposed design is a semicircular-shaped antenna with a semicircular-shaped cut at the top edge. The rectangular and triangular slots at the ground plane achieve good impedance match in the UWB range. For gain enhancement, single-layered FSS reflector is employed. Tested and simulated results ascertain that the presented antenna with frequency-selective surface (FSS) attains a gain improvement of average 4 dB. Thus, the compactness, simple structure, high gain, and UWB spectrum validate the suitability of the reported radiating element for the modern communication systems.

2. Geometry and Characterization of Antenna

2.1. Design Procedure of Antenna. Figure 1 depicts the layout of the presented design. The initial geometry consists of a rectangular patch antenna extended into circular shape with a semicircular-shaped slit at the upper edge in the center. The back side of the substrate consists of a partial ground which is further optimized by etching a rectangular and two triangular-shaped slits to attain the UWB characteristics. The proposed antenna for UWB applications is modeled using the easily accessible FR4 substrate having thickness of 1.6 mm, relative permittivity (ϵr) of 4.4, and loss tangent (tan δ) of 0.02, where the overall substrate dimensions are $Ls \times Ws$. The antenna is excited through microstrip feed to deliver maximum power to the radiating patch. Modeling and designing of the structure is performed using CST Microwave Studio. Various parameters are optimized to obtain the optimal radiation performance of the radiating patch. Table 1 provides the design values of the final reported design.

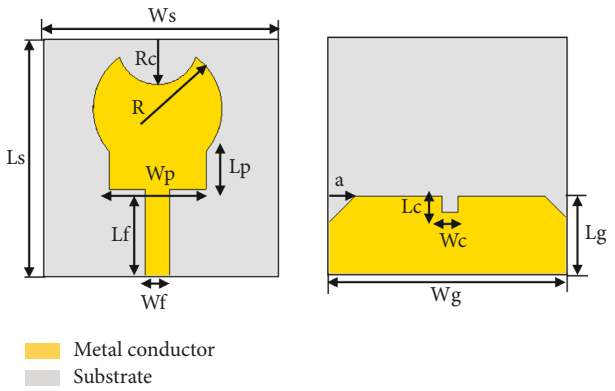

Figure 1: Layout of the reported antenna.

Table 1: Optimized values of reported design (mm).

Parameter	Value (millimetre)
Lf	11.05
Wf	3
Wp	12
Lp	8
R	8
Lg	10
Ls	30
Lc	2
Wc	2
W g	30
Hc	0.035
a	3
Ws	30
Rc	5

2.2. Design Methodology. The overall design process to obtain the final optimized antenna consists of three stages, as illustrated in Figures 2(a)–2(c). At the first stage, a rectangular-shaped patch antenna is obtained using the well-established equation (34). The bottom layer of substrate is partial, as illustrated in Figure 2(a). The rectangular antenna resonates for the wide frequency band ranging from 4.2 to 11 GHz, as depicted by the reflection coefficient results in Figure 2(d). This antenna attained peak gain value of 3.9 dB for the resonant band, as illustrated in Figure 3. In the next stage, a circular-shaped patch is integrated with the previously designed antenna such that the design evolves in to a bulb-shaped antenna, as depicted in Figure 2(b). The effective radius (Re) of the circular patch can be calculated with the help of equation(3) [34].

$$w = \frac{vo}{2fr}\sqrt{\frac{2}{\epsilon_r}}, \tag{1}$$

$$L = \frac{vo}{2fr\sqrt{\epsilon_{eff}}} - 2\Delta L, \tag{2}$$

$$R_e = R\left\{\sqrt{1 + \frac{2H}{\pi\epsilon_r R}\left(\ln\frac{\pi R}{2H} + 1.7726\right)}\right\}. \tag{3}$$

The effective radius (Re) of the circular patch can be calculated with the help of equation (1). The calculated effective radius (Re) of proposed antenna is 8.5 mm which is approximately equal to the parametric value, i.e., 8 mm. Here H is the thickness of the substrate, ϵ_r is the relative permittivity, and R is the physical radius of the antenna which could be calculated in terms of resonate frequency using the following relation [34]:

$$R = \frac{F}{\left\{\sqrt{1 + 2h/\pi\epsilon_r F\left(In\ \pi F/2H + 1.7726\right)}\right\}}, \tag{4}$$

where F can be estimated using the following equation:

$$F = \frac{8.79 \times 10^9}{fr\sqrt{\epsilon_r}}. \tag{5}$$

This antenna attained impedance bandwidth of 3–11 GHz. Thus, widening of the band is observed at this stage. In addition to bandwidth enhancement, the peak antenna gain attained is 4.1 dB. Later, the design is modified by making a semicircular cut at the top center of the antenna as well as one rectangular and two triangular slots from the ground layer, as depicted in Figure 2(c). It is noted that the antenna gain further enhances to 5 dB. Also, the impedance matching improves as the reflection coefficient curve slightly shifts towards lower values, as exhibited by reflection coefficient results in Figure 2(d).

3. Design of Frequency-Selective Surface (FSS)

3.1. Unit Cell Design. Literature review shows that FSS is an eminent technique to improve the antenna gain. The structure design process of the FSS starts with unit cell. The primary factors affecting the performance of the FSS include unit cell size, geometry, spacing between the unit cells, dielectric thickness, and so on. Initially, a square-shaped structure with circular slot is obtained as unit element through optimization, as shown in Figure 4(a). Through the analysis of the response of this unit cell exhibited in Figure 4(c), it is observed that the resonant frequency band ranges from 3 to 5.5 GHz. Afterwards, the unit cell is modified by incorporating a vertical conducting strip in the center of the circular slot such that the circular slot is divided into two semicircular slots. The response obtained by this modified unit cell ranges between 2.8 and 6.4 GHz. Later, in order to obtain the wideband response, the geometry of the unit cell is further modified by employing a horizontal conducting strip, as depicted in Figure 4(a). Thus, the final unit cell design consists of a square-shaped structure with two conducting strips placed in the center making a plus (+) shape. It is noticed that the final unit cell obtains the wideband frequency response ranging from 3.3 to 10.5 GHz, thus attaining good attenuation stop-band characteristics in this frequency band. Figure 4(b) exhibits the port assignment and boundary conditions to excite the unit cell, whereas the parametric values of the optimized unit cell are provided in Table 2.

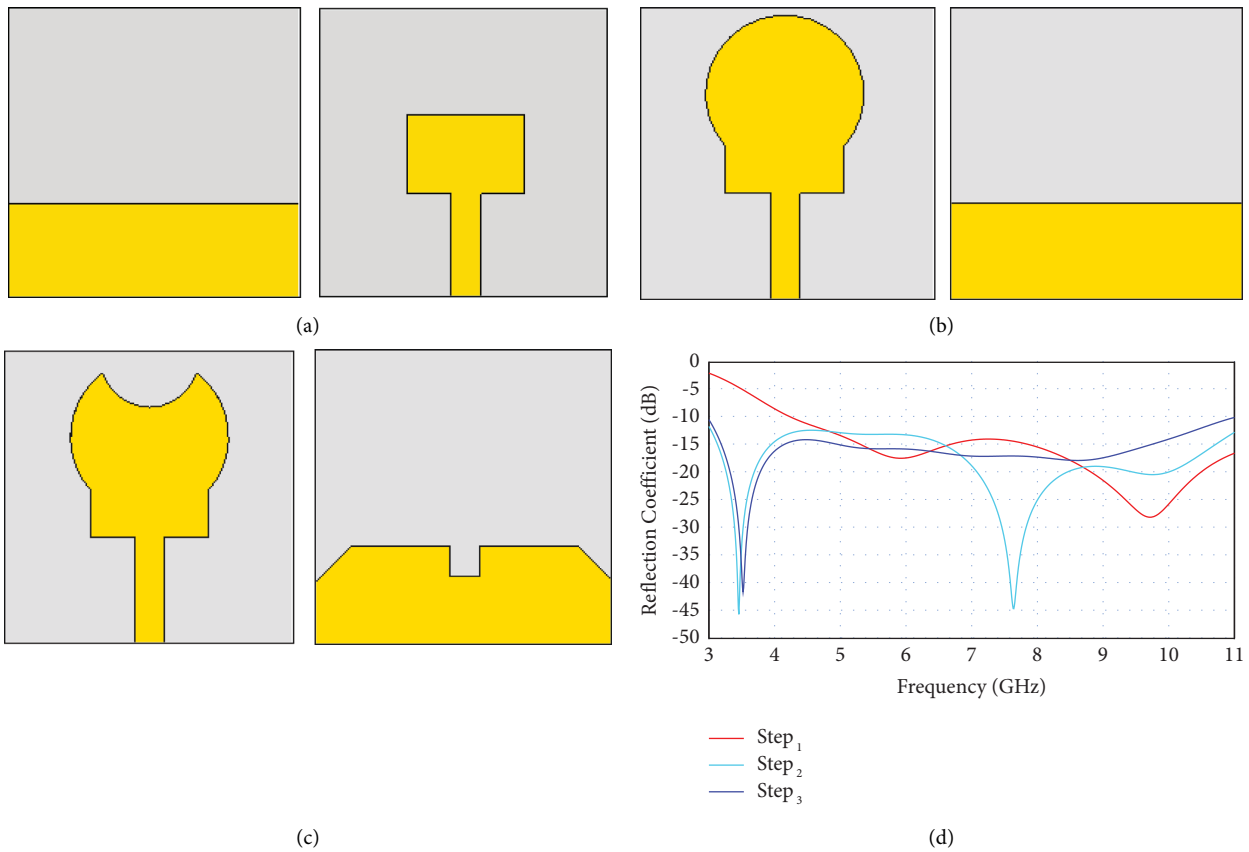

Figure 2: (a–c) Stepwise antenna design progress. (d) Simulated reflection coefficient for all design steps.

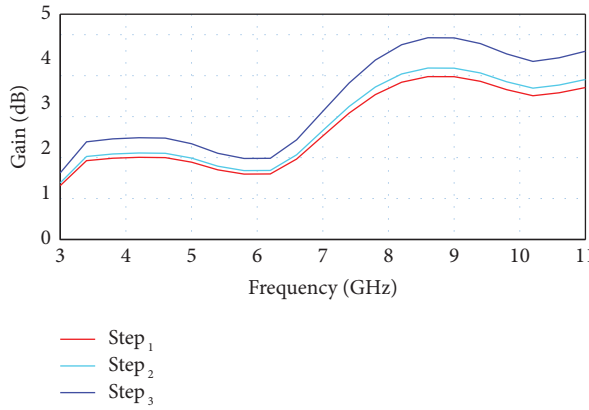

Figure 3: (a–c) Stepwise antenna design frequency vs. gain for all design steps.

3.2. EC Model of Unit Cell. An equivalent circuit model for proposed unit cell, as shown in Figure 5(a), is designed and simulated in Advanced Design System (ADS) software, which provides an equivalent impedance bandwidth of the FSS unit cell. The equivalent circuit consists of resistor-inductor-capacitor (RLC) circuit, where inductors are connected in parallel, while capacitors and resistors are connected in series, as depicted in Figure 5(a). The 0.2 ohm resistors are representing the resistance of conducting material, the inductors ($L14$, $L15$, $L16$, $L17$, $L18$, $L19$, $L20$, and $L21$) are representing the conducting portion of unit cell, and the capacitors ($C6$, $C11$, $C13$, and $C15$) are representing the cuts/air gap among adjacent conductors inside the unit cell. Moreover, capacitors ($C9$, $C10$, $C14$, and $C14$) are representing the separation among the adjacent unit cells. The desired results similar to CST are obtained by tuning the values of inductors and capacitors [35]. The required inductance and capacitance can be calculated using equations (6) and (7) [36], as provided below.

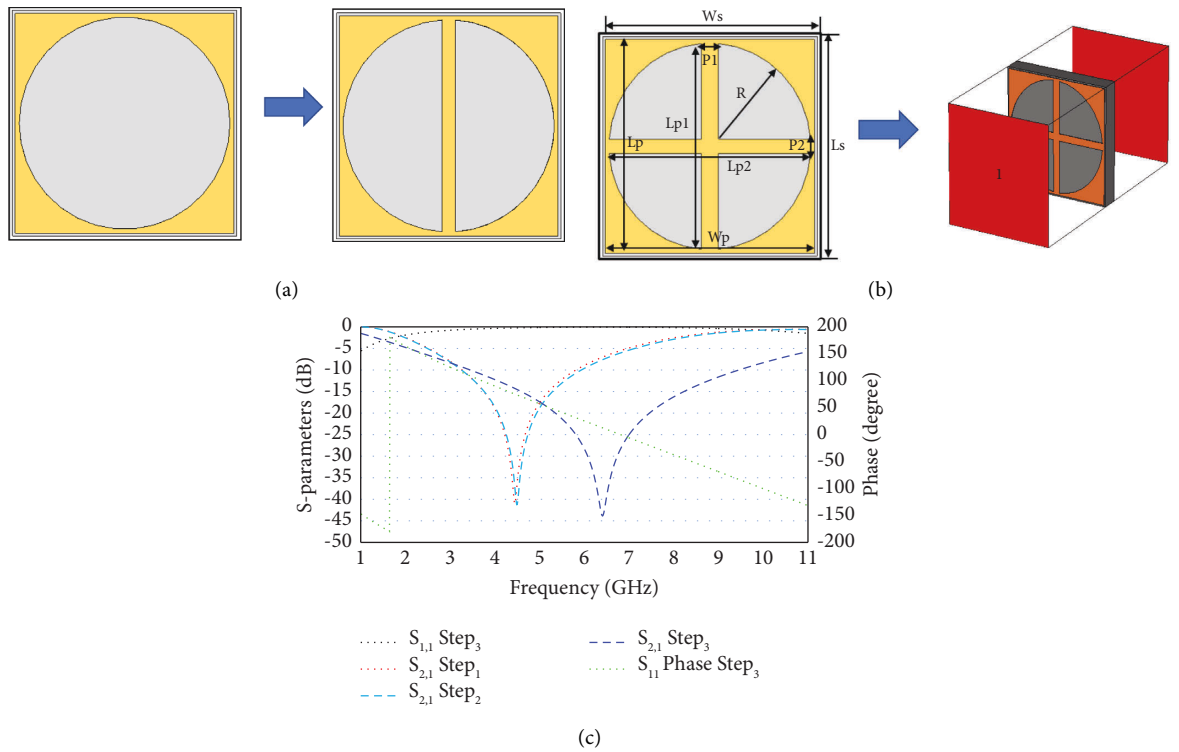

Figure 4: (a) Unit cell steps. (b) Unit cell excitation. (c) S parameters.

Table 2: Design parameters of reported unit cell.

Parameter	Value (millimetre)
L_s	10
w_s	10
L_p	9.75
w_p	9.75
l_p	0.6
P_2	9.75
R	4.7
H_s	1.6
Lp_2	9.4
Lp_1	9.4

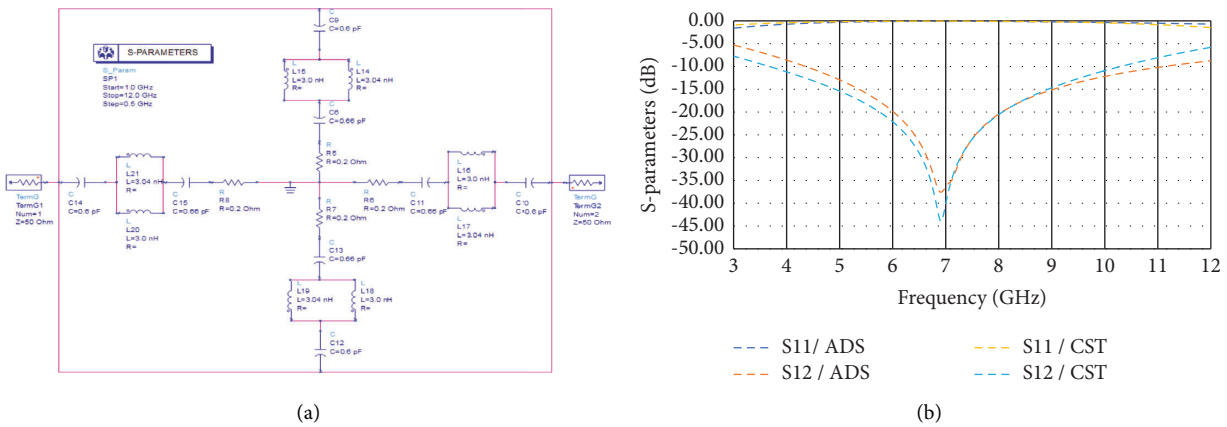

Figure 5: (a) EC associated with unit cell. (b) Transmission coefficient of unit cell.

$$\frac{X_L}{Zo} = \frac{d}{p} F(P, w, \lambda, \theta) = \frac{d}{\lambda} \cos\theta \left[\ln\left(\csc\left(\frac{\pi w}{2p} \right) \right) + G(P, w, \lambda, \theta) \right], \tag{6}$$

$$\frac{B_C}{Y_o} = 4\frac{d}{p} F(P, g, \lambda, \theta)\epsilon_{eff} = 4\frac{d}{p} \sec\theta \left[\ln\left(\csc\left(\frac{\pi g}{2p} \right) \right) + G(p, g, \lambda, \theta) \right] \epsilon_{eff}. \tag{7}$$

As the proposed unit cell is designed for UWB bandwidth stop response, the transmission coefficient of unit cell must be lower than −10 dB for the operating band ranging from 3.1 to 10.6 GHz to achieve UWB stop response. The transmission coefficient plots for the proposed unit cell obtained by using CST and ADS show good agreement, as presented in Figure 5(b).

3.3. Performance Analysis of FSS Loaded Antenna

3.3.1. Performance Analysis with Different Array Configurations. The geometrical structure of the optimized reported antenna loaded with FSS is illustrated in Figure 6. The final proposed FSS comprises 36 elements arranged in 6×6 (rows×columns) order along with antenna placed above it at height H. The substrate used for this FSS structure is FR4 with 1.6 mm thickness. The dimension of the FSS is 62.5× 62.5×1.6mm^3. In order to get the optimal antenna performance, an investigation is carried out on the effects of varying the FSS size on the antenna radiation characteristics. The analysis is conducted for different array arrangements with 4×4, 5×5, and 6×6 unit cell elements placed at same distance of 20 mm from the antenna, as depicted in Figure 6(a). It is noticed that antenna shows good impedance matching with 6×6 FSS array, as evident by the reflection coefficient plots illustrated in Figure 6(b) that an improved impedance matching is obtained. In addition, Figure 6(c) depicts that antenna gain also improves with increasing number of unit cells, where peak gain of 7.5 dBi is obtained for 6×6 unit cell configuration.

The size of antenna limits the size of FSS unit cells. Here is investigated in-depth study of the influence of the proposed FSS unit cell dimension on the given reported radiating element. It is observed that by increasing the number of unit cells, the impedance bandwidth and gain of proposed antenna are improved [37].

3.3.2. Performance Analysis with Different Gap Values between Antenna and FSS. The requirement of FSS for antenna applications is to design such FSS surface which has the same bandwidth as the proposed antenna, i.e., for UWB antenna, the FSS and antenna should have the bandwidth ranging from 3.1 to 10.6 GHz. The reported antenna is integrated with ultra-wide stop-band FSS, as depicted in Figure 6(a). To reduce the coupling between antenna and FSS surface, the FSS must be placed at a distance $\lambda/2$ at the transmitting and receiving antenna. When the antenna is integrated at specific distance on the FSS, the FSS reflected the backward radiation of the antenna. This reflected wave is directed to the opposite side of the FSS surface. Therefore, two wave components will be added in the same phase and given us constructive interference and improved radiation gain. If ϕt and ϕr are the phases of the antenna's transmitted and reflected waves, then the complete propagation trip between FSS is denoted by ϕs.

$$\phi t = \phi r + \phi s \text{ and } \phi\, s = 2 \times 2\pi f \times \frac{g}{c}, \tag{8}$$

where c is the speed of light, g is gap between antenna and metallic reflector, and ϕt should be 0 or integral of 2π [30]. In this proposed work, the FSS is employed beneath the radiating element so that the back radiation of the antenna should be reflected. So, the FSS makes the back radiation of antenna in phase and then the antenna gain enhances. In this scenario, an important factor is the space among the reference antenna and the FSS surface, which ensures the constructive interference of directly radiated and reflected waves. In order to estimate the spacing between the FSS and antenna, the following equation is used [27]:

$$\phi_{Fss} - 2\beta H = 2n\pi \text{ where } n = \ldots -1, 0, 1 \ldots, \tag{9}$$

where π represents the phase of reflected wave from FSS layer and H is the gap between the antenna and FSS, whereas β is open space propagation wave consonant. The spacing between the antenna and the FSS layer must be an integer multiple of the wavelength at the central frequency. However, due to the wideband nature of FSS, the gap between the FSS layer and antenna is optimized such that the maximum gain is achieved. Therefore, a parametric investigation is performed for gap between the radiating element and the optimized FSS layer with 6×6 element array. For the initial distance of 14 mm, peak gain of 8.5 dBi is obtained, as depicted in Figure 7, whereas for the gap of 17 mm and 20 mm, the antenna gain reduces with maximum values at 7.5 and 7.2 dB. Hence, it is noticed that antenna gain is maximum at spacing of 14 mm between FSS and antenna. Thus, the final proposed design with optimal performance is an UWB antenna with 6×6 FSS layer employed beneath antenna at a space of 14 mm.

4. Experimental Results

In order to validate the performance of the proposed antenna, prototype is fabricated as shown in Figure 8 and measured experimentally. The VNA Network Analyzer N5224A is used to measure the S-parameters of the antenna, whereas the far-field characteristics are measured by anechoic chamber in the National University of Science and Technology (NUST). The measured results obtained are well

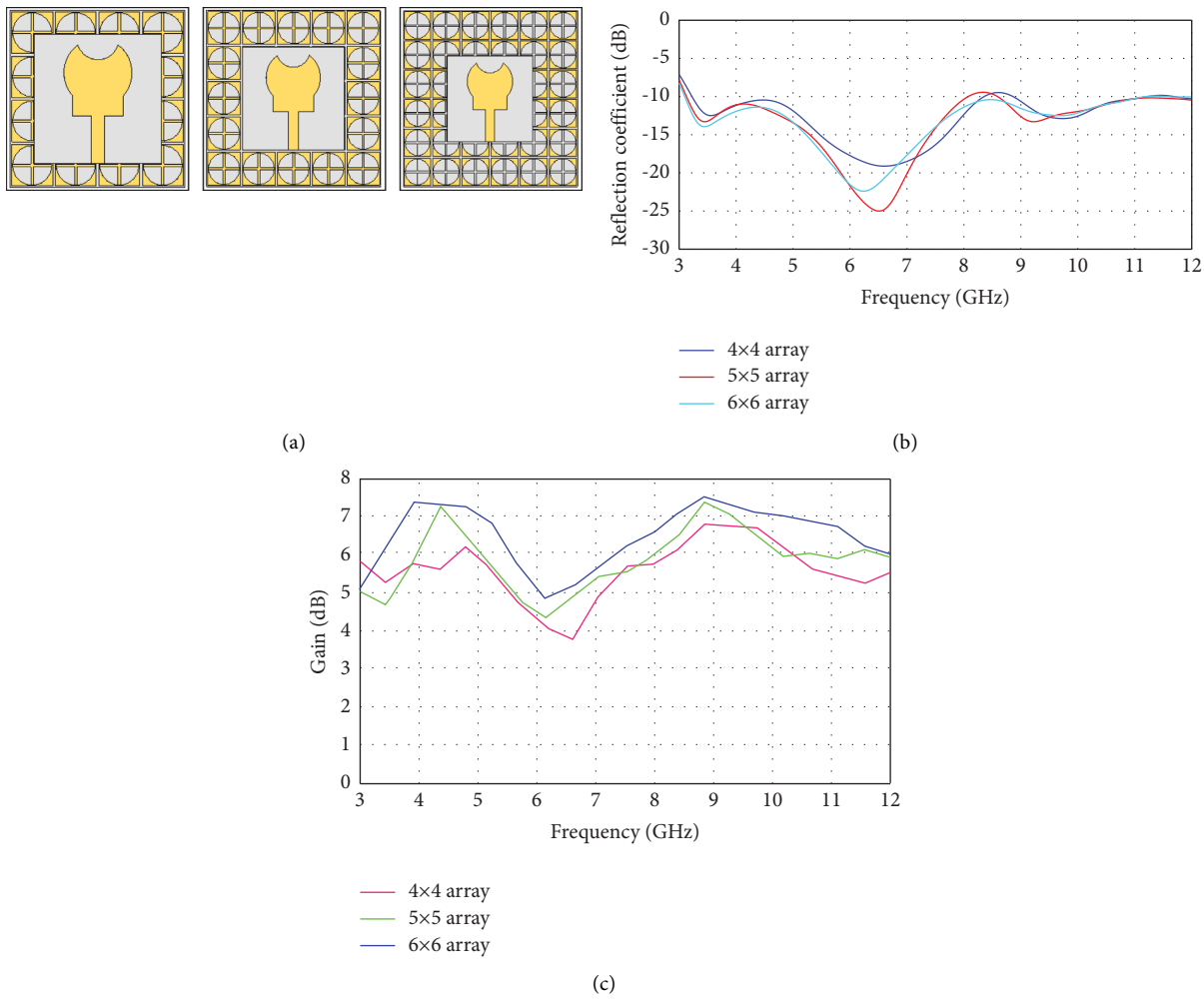

Figure 6: (a) FSS array configurations. (b) Reflection coefficient for FSS arrays. (c) Simulated antenna gain for FSS arrays.

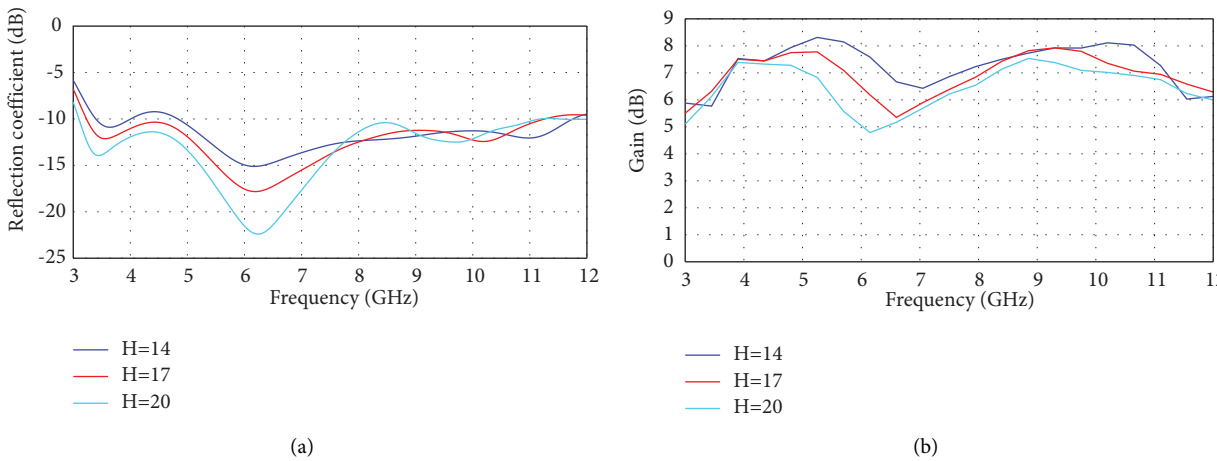

Figure 7: Simulated (a) reflection coefficient and (b) gain with different gap values between FSS and antenna.

matched with the simulated results; however, few discrepancies were found due to imperfections in fabrication and tolerance in the measurement setup.

4.1. Reflection Coefficient. Figure 9 exhibits the simulated and measured reflection coefficient (*S*11) of the antenna with and without FSS configurations. The measured results of the

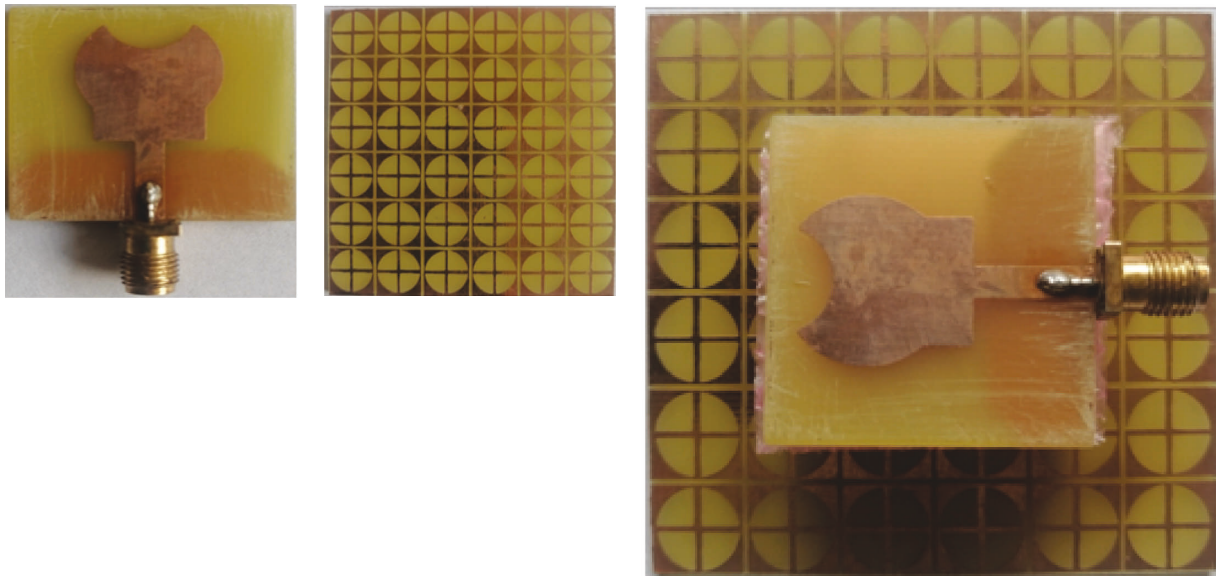

(a) (b) (c)

Figure 8: Fabricated prototypes for the following: (a) UWB antenna, (b) FSS reflector, and (c) UWB with FSS reflector.

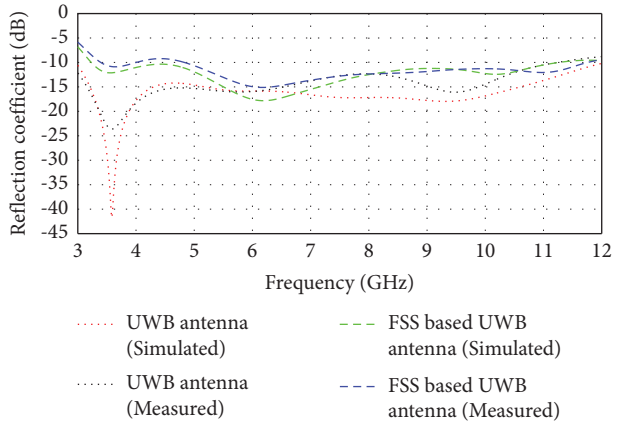

Figure 9: Tested and simulated reflection coefficient ($S11$) of antenna with and without FSS.

proposed antenna without FSS demonstrate that the antenna shows good impedance matching and resonates for the frequency band ranging from 3 to 11 GHz, thus covering the UWB. Moreover, when antenna is measured with FSS placed below it, a slight upward and a minor forward shift is observed for the obtained band ranging from 3.3 to 11.5 GHz. This is due to fabrication loss and connector loss during measurement. However, obtained band still covers the UWB. It is also noted that measured and simulated results have good coherence, and insignificant differences occur mainly due to fabrication errors and tolerance in the measurement equipment.

4.2. Far-Field Results. The far-field measurements are obtained in anechoic chamber. Figures 10(a)–10(c) demonstrate the simulated and measured radiation patterns for E and H planes at 3.1, 5.3, and 9 GHz. It is observed that for all selected frequencies, the antenna exhibits a bidirectional radiation pattern, whereas an omnidirectional radiation pattern is obtained for the principal H-plane. Simulated and measured results show good agreement. Moreover, simulated and measured gain of the proposed UWB antenna with and without FSS is depicted in Figure 11. It is observed that an enhancement of nearly 4 dB gain is obtained after the employment of FSS below the antenna, where the peak measured gain is 8 dB at 5.5 GHz.

4.3. Efficiency. It is observed that if we increase frequency, the radiation becomes more directive and gain of the radiating element also increases. In addition to improvement in gain, the efficiency of antenna also improves and a maximum efficiency of 80% is attained at 9 GHz. Moreover, when FSS is employed below the antenna, the efficiency improves and achieves a maximum efficiency of 87% at the

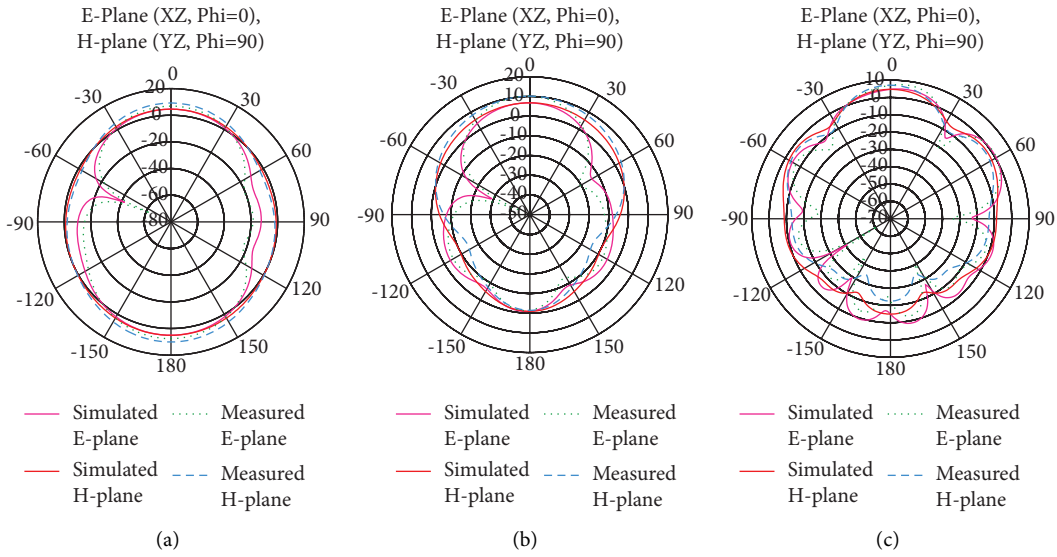

Figure 10: *E*-plane and *H*-plane of FSS-based UWB antenna at (a) 3.1 GHz, (b) 5.3 GHz, and (c) 9 GHz.

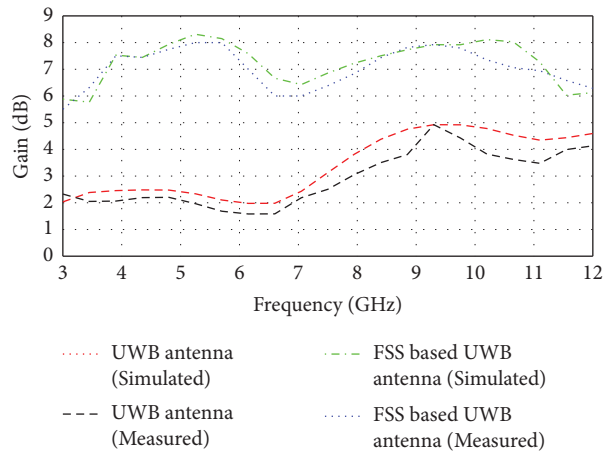

Figure 11: Tested and theoretical gain (dB) of antenna with and without FSS.

same frequency. Measured results show close agreement with simulated results, as depicted from the antenna efficiency plots in Figure 12.

5. Comparison with Related Work

This section provides the comparative analysis of the proposed UWB antenna with some other related works published recently. This comparison is summarized in Table 3, considering key design and performance metrics. The works reported in [29, 30] are UWB antennas where single-layered FSSs are employed to enhance gain. The reported structures with overall dimensions of $84 \times 84 \times 1.6\,\text{mm}^3$ and $33 \times 33 \times 1.6\,\text{mm}^3$attained peak gain of 8.7 dB and 7.9 dB, respectively. On the other hand, UWB antennas presented in [26, 34, 37–41] introduced double-layered FSS for gain enhancement. A wideband and high-gain microstrip antenna with H-shaped resonator insertion is presented in this paper for self-powered wireless Wi-Fi applications. The impedance bandwidth of the proposed antenna below −10 dB ranges from 3 GHz up to 7.43 GHz. After the inclusion of HSR (*H*-shaped resonator), the gain is improved between 9.52 dB and 16.71 dB [42]. A miniaturized UWB microstrip antenna with slotted patch is design for UWB communication. Then, H-shaped metamaterial resonators are inserted on the top of substrate for bandwidth enhancement [43]. It is evident from Table 3 that most of these proposed structures have larger dimensions as compared to the design proposed in this work. Also, the peak gain obtained is comparatively low for most of these reported antennas. Moreover, these structures are bulky and have high fabrication complexity due to dual FSS layers. Conversely, the antenna design proposed in this work is a simple UWB antenna with single layer of FSS which reduces the fabrication complexity of the design. Also, the peak gain

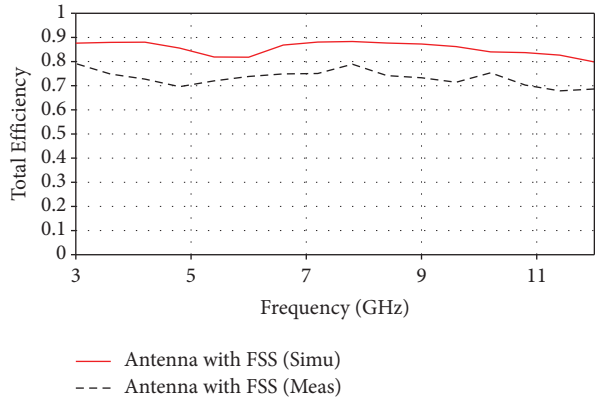

Figure 12: Total efficiencies of proposed antenna with FSS.

Table 3: Comparison of FSS-based antenna with previous work.

Ref no.	Dimension of antenna (millimetre)	Dimension of FSS (millimetre)	Peak gain (dB)	Bandwidth (GHz)	FSS surface
[26]	30 ×60 × 0.7	75 ×105 × 1.6	8	3–11.6	Dual
[29]	20 ×27 × 1.6	84 ×84 × 1.6	8.7	4.7–14.9	Single
[30]	30 × 31.9 × 1.6	33 × 33 × 1.6	7.9	2.6–11.9	Single
[34]	25 ×31 × 1.5	90 ×60 × 25	7	3–10	Dual
[38]	10 ×12 × 0.8	102 ×102 × 1.6	9.5	3–10	Dual
[39]	25 ×25 × 1.6	124 ×124 × 1.6	8.2	6.5–9.5	Dual
[37]	45 ×45 × 1.6	45 ×45 × 1.6	3.2	3–12	Dual
[40]	28 ×34 × 1.6	150 ×150 × 30	7.5	3–10.6	Dual
[41]	38.3 ×34.5 × 1.6	44 ×44 × 1.6	6	2–11	Dual
[42]	60 × 60	—	16.71	1.75–7.43	Metamaterial inserted
[43]	60 × 30	—	—	3–10	Metamaterial inserted
Proposed	30 ×30 × 1.6	62.5 ×63 × 25	8.3	3–12	Single

obtained is higher as compared to most of the literary works reported recently.

6. Conclusion

A novel circular-shaped antenna with a semicircular slot at the top side with frequency-selective surface (FSS) layer is reported in this work. The FSS enhances the antenna gain across the whole UWB bandwidth and improves directivity of the radiating element. In addition, the reported unit cell having dimension of $0.11\,\lambda \times 0.11\,\lambda$ is designed for UWB application, achieving the stop-band response over the entire UWB spectrum. Whereλ presents the wavelength based on the lowest operational frequency, i.e. 3.3 GHz, and it attains stop band of 7.2 GHz across 3.3–10.5 GHz. This article shows that FSS enhances the gain of UWB antenna from 2.3 dB to 8.3 dB at 5.3 GHz and improves average gain of 4 dB in the whole band. The compact and low-profile FSS-based antenna is useful for UWB and ground-penetrating radar (GPR) application. Furthermore, we can notch some existing bands in the UWB spectrum, i.e., WiMAX, WLAN, and ITU bands, to avoid interference, then we can make the notches reconfigurable, and design UWB antenna for WBAN application and metamaterial-based UWB antenna for energy harvesting purpose.

Data Availability

The data used to support the findings of this study are included within the article.

Conflicts of Interest

The authors declare that they have no conflicts of interest.

Acknowledgments

Dr. Mohammad Alibakhshikenari acknowledges support from the CONEX-Plus programme funded by Universidad Carlos III de Madrid and the European Union's Horizon 2020 research and innovation programme under the Marie Sklodowska-Curie grant agreement No. 801538.

References

[1] G. R. Aiello and G. D. Rogerson, "Ultra-wideband wireless systems," *IEEE Microwave Magazine*, vol. 4, no. 2, pp. 36–47, 2003.

[2] K. Siwiak and D. McKeown, *Ultra-wideband Radio Technology"*, John Wiley & Sons, no. 9, , p. 193, Chichester, UK, 2004.

[3] J. H. Reed, *An Introduction to Ultra-wideband Communication Systems*, pp. 1–50, Prentice Hall Press, Hoboken, NJ, USA, 2005.

[4] M. A. Jamlos, M. F. Jamlos, S. Khatun, and A. H. Ismail, "A compact super wide band antenna with high gain for medical applications," in *Proceedings of the IEEE Symposium on Wireless Technology and Applications (ISWTA)*, Kota Kinabalu, Malaysia, September 2014.

[5] W. S. Yeoh and W. S. T. Rowe, "An UWB conical monopole antenna for multiservice wireless applications," *IEEE Antennas and Wireless Propagation Letters*, vol. 14, no. 1, pp. 1085–1088, 2015.

[6] R. V. S. R. Krishna and R. Kumar, "A dual-polarized square-ring slot antenna for UWB, imaging, and radar applications," *IEEE Antennas and Wireless Propagation Letters*, vol. 15, no. c, pp. 195–198, 2016.

[7] J. Ali, N. Abdullah, M. Yusof, E. Mohd, and S. Mohd, "Ultra-wideband antenna design for GPR applications: a review," *International Journal of Advanced Computer Science and Applications*, vol. 8, no. 7, pp. 392–400, 2017.

[8] A. Musavand, "A compact UWB slot antenna with reconfigurable band-notched function for multimode applications," *Applied Computational Electromagnetics Society Journal*, vol. 13, no. 1, pp. 975–980, 2016.

[9] A. M. Abbosh and M. E. Bialkowski, "Design of ultra-wideband planar monopole antennas of circular and elliptical shape," *IEEE Transactions on Antennas and Propagation*, vol. 56, no. 1, pp. 17–23, 2008.

[10] J. Liu, S. Zhong, and K. P. Esselle, "A printed elliptical monopole antenna with modified feeding structure for bandwidth enhancement," *IEEE Transactions on Antennas and Propagation*, vol. 59, no. 2, pp. 667–670, 2011.

[11] M. Ojaroudi, C. Ghobadi, and J. Nourinia, "Small square monopole antenna with inverted T-shaped notch in the ground plane for UWB application," *IEEE Antennas and Wireless Propagation Letters*, vol. 8, pp. 728–731, 2009.

[12] Y. Lu, Y. Huang, H. T. Chattha, and P. Cao, "Reducing ground-plane effects on UWB monopole antennas," *IEEE Antennas and Wireless Propagation Letters*, vol. 10, pp. 147–150, 2011.

[13] K. Xu, Z. Zhu, H. Li, J. Huangfu, C. Li, and L Ran, "A printed single-layer UWB monopole antenna with extended ground plane stubs," *IEEE Antennas and Wireless Propagation Letters*, vol. 12, pp. 237–240, 2013.

[14] M. G. N. Alsath and M. Kanagasabai, "Compact UWB monopole antenna for automotive communications," *IEEE Transactions on Antennas and Propagation*, vol. 63, no. 9, pp. 4204–4208, 2015.

[15] A. Dastranj and F. Bahmanzadeh, "A compact UWB antenna design using rounded inverted L- shaped slots and beveled asymmetrical patch," *Progress In Electromagnetics Research C*, vol. 80, pp. 131–140, 2018.

[16] A. Bekasiewicz and S. Koziel, "Structure and computationally efficient simulation-driven design of compact UWB monopole antenna," *IEEE Antennas and Wireless Propagation Letters*, vol. 14, pp. 1282–1285, 2015.

[17] S. Koziel and A. Bekasiewicz, "A structure and simulation-driven design of compact CPW-fed UWB antenna," *IEEE Antennas and Wireless Propagation Letters*, vol. 15, pp. 750–753, 2016.

[18] J. Tao and Q. Feng, "Compact ultra-wideband MIMO antenna with half-slot structure," *IEEE Antennas and Wireless Propagation Letters*, vol. 16, pp. 792–795, 2017.

[19] F. Fereidoony, S. Chamaani, and S. A. Mirtaheri, "UWB monopole antenna with stable radiation pattern and low transient distortion," *IEEE Antennas and Wireless Propagation Letters*, vol. 10, pp. 302–305, 2011.

[20] G. K. Pandey, H. S. Singh, and P. K. Bharti, "UWB monopole antenna with enhanced gain and stable radiation pattern using gate like structures," in *Proceedings of the Int.Conf. Microwave Photonics, ICMAP*, pp. 4–7, Dhanbad, India, December 2013.

[21] K. S. Ryu and A. A. Kishk, "UWB dielectric resonator antenna having consistent omnidirectional pattern and low cross-polarization characteristics," *IEEE Transactions on Antennas and Propagation*, vol. 59, no. 4, pp. 1403–1408, 2011.

[22] J. Wang and Y. Yin, "Differential-fed UWB microstrip antenna with improved radiation patterns," *Electronics Letters*, vol. 50, no. 20, pp. 1412–1414, 2014.

[23] T. H. Hsieh and C. S. Lee, "Double-layer high-gain microstrip array antenna," *IEEE Transactions on Antennas and Propagation*, vol. 48, no. 7, pp. 1033–1035, 2000.

[24] R. Ram Krishna, R. Kumar, Slotted ground microstrip antenna with FSS reflector for high-gain horizontal polarisation," *Electronics Letters*, vol. 51, no. 8, pp. 599-600, 2015.

[25] G. Sen, A. Banerjee, M. Kumar, and S. Das, "An ultra-wideband monopole antenna with a gain enhanced performance using a novel split-ring meta-surface reflector," *Microwave and Optical Technology Letters*, vol. 59, no. 6, pp. 1296–1300, 2017.

[26] S. Kundu, A. Chatterjee, S. K. Jana, and S. K. Parui, "Gain enhancement of a printed leaf shaped UWB antenna using dual FSS layers and experimental study for ground coupling GPR applications," *Microwave and Optical Technology Letters*, vol. 60, no. 6, pp. 1417–1423, 2018.

[27] Y. Yuan, X. Xi, and Y. Zhao, "Compact UWB FSS reflector for antenna gain enhancement," *IET Microwaves, Antennas & Propagation&Propagation*, vol. 13, no. 10, pp. 1749–1755, 2019.

[28] S. Kundu, "A compact uniplanar ultra-wideband frequency selective surface for antenna gain improvement and ground penetrating radar application," *International Journal of RF and Microwave Computer-Aided Engineering*, vol. 30, no. 10, Article ID e22363, 2020.

[29] R. A. Abdulhasan, R. Alias, K. N. Ramli, F. C. Seman, and R. A. AbdAlhameed, "High gain CPW-fed UWB planar monopole antenna-based compact uniplanar frequency selective surface for microwave imaging," *International Journal of RF and Microwave Computer-Aided Engineering*, vol. 29, no. 8, Article ID e21757, 2019.

[30] P. Das, K. Mandal, Modelling of ultra-wide stop-band frequency-selective surface to enhance the gain of a UWB antenna," *IET Microwaves, Antennas & Propagation & Propagation*, vol. 13, no. 3, pp. 269–277, 2019.

[31] N. Melouki, A. Hocini, and T. A. Denidni, "Performance enhancement of an ultra-wideband antenna using a compact topology optimized single frequency selective surface-layer as a reflector," *International Journal of RF and Microwave Computer-Aided Engineering*, vol. 32, no. 5, Article ID e23097, 2022.

[32] K. Nishanth Rao and V. Meshram, H. N. Suresh, SSA based microstrip patch antenna design with FSS for UWB application," *Wireless Personal Communications*, vol. 123, no. 3, pp. 2533–2553, 2022.

[33] S. Kundu, "High gain compact ultra-wideband "antenna-frequency selective surface" and its performance evaluation in

proximity of soil surface," *Microwave and Optical Technology Letters*, vol. 63, no. 3, pp. 869–875, 2021.

[34] G. Sen, A. Banerjee, M. Kumar, and S. Das, "An ultra-wide band monopole antenna with a gain enhanced performance using anovel split-ring meta-surface reflector," *Microwave and Optical Technology Letters*, vol. 59, no. 6, pp. 1296–1300, 2017.

[35] T. Hussain, Q. Cao, J. K. Kayani, and I. Majid, "Miniaturization of frequency selective surfaces using 2.5-d knitted structures: design and synthesis," *IEEE Transactions on Antennas and Propagation*, vol. 65, no. 5, pp. 2405–2412, 2017.

[36] S. Bijimanzil Abdulkareem and S. Gopalakrishnan, "Modelling of a polarization-insensitive UWB FSS with bandstop response," *Radio Engineering*, vol. 30, no. 2, pp. 342–348, 2021.

[37] M. Daghari and H. Sakli, "Radiation performance enhancement of an ultra wide band antenna using metamaterial bandpass filter," *International Journal of Electrical and Computer Engineering (IJECE) & Computer Engineering*, vol. 10, no. 6, pp. 2088–8708, 2020.

[38] Y. Ranga, L. Matekovits, K. P. Esselle, and A. R. Weily, "Multioctave frequency selective surface reflector for ultrawideband antennas," *IEEE Antennas and Wireless Propagation Letters*, vol. 10, pp. 219–222, 2011.

[39] R. Saleem, M. Bilal, T. Shabbir, and M. F. Shafique, "An FSS-employed UWB antenna system for high-gain portable devices," *Microwave and Optical Technology Letters*, vol. 61, no. 5, pp. 1404–1410, May 2019.

[40] R. Kumar and N. Kushwaha, "On the design of linear to circular polarization converter based on fss," in *Proceedings of the 2020 International Conference on Electrical and Electronics Engineering (ICE3)*, pp. 101–104, Gorakhpur, India, February 2020.

[41] S. Kundu and A. Chatterjee, "Sharp triple-notched ultra wideband Antenna with gain augmentation using FSS for ground penetrating radar," *Wireless Personal Communications*, vol. 117, no. 2, pp. 1399–1418, 2021.

[42] A. Abdulmjeed, T. A. Elwi, and S. Kurnaz, "Metamaterial Vivaldi printed circuit antenna based solar panel for self-powered wireless systems," *Progress In Electromagnetics Research M*, vol. 102, pp. 181–192, 2021.

[43] A. Abdulmjeed, T. A. Elwi, and S. Kurnaz, "A miniaturized UWB microstrip antenna structure," 2018, https://www.scitcentral.com/article/39/281/A-Mini.